Samarra Journal of Pure and Applied Science

www.sjpas.com

p ISSN: 2663-7405
e ISSN: 2789-6838

An Intelligent Health Informatics Framework for Automated Brain Tissue Segmentation in MRI Using U-Net-Based Convolutional Neural Networks

Mohanad F. Jwaid

Al-Hadara University college, Iraq

https://doi.org/10.54153/sjpas.2026.v8i1.1393

Article Information

Received: 09/01/2026
Revised: 20/02/2026
Accepted: 15/03/2026
Published: 10/04/2026

Keywords:

Brain MRI, Tissue Segmentation, U-Net, Convolutional Neural Networks, Medical Image Analysis, Deep Learning.

Corresponding Author

E-mail:
Mohanad02jwaid@gmail.com
Mobile:

Abstract

This study proposes an intelligent framework for automated brain tissue segmentation in MRI scans using U-Net-based convolutional neural networks, aiming to improve accuracy over existing methods. The methodology involves implementing both 2D and 3D U-Net architectures, trained and validated on public datasets (MRBrainS13, MRBrainS18, IBSR) with manual expert segmentations. Performance was compared against established tools (FSL, Dipy) using Dice Coefficient, Jaccard Index, AUC, and SSIM metrics. Results demonstrate the superiority of U-Net models, with Dice scores exceeding 0.9 for gray matter and showing high consistency, while 2D U-Net slightly outperformed the 3D variant in reducing false positives and negatives. The conclusion confirms that U-Net-based segmentation significantly enhances precision and reliability for distinguishing gray matter, white matter, and cerebrospinal fluid, offering a robust alternative to conventional techniques

Introduction:

Malformations in brain structure refer to alterations in the shape, size, or position of the brain structure, which can affect a person's neurological function and overall health [1]. These alterations can develop in an embryonic stage (congenital malformations) or be acquired throughout life. Congenital structural changes are usually due to a disruption in the normal development of the embryonic or fetal stage, while acquired malformations usually correspond to diseases, injuries, environmental circumstances, or other external causes [2]. In general, this type of condition leads to diseases such as refractory epilepsy caused by cortical dysplasias, considered the main cause of this disease, Alzheimer's due to contractions in brain regions, multiple sclerosis due to brain volume loss, microangiopathy caused by Virchow-Robin spaces and in the case of malformations such as Chiari, multiple symptoms may appear

such as imbalance, tinnitus, difficulty swallowing, palpitations, sleep apnea, muscle weakness, chronic fatigue, and painful tingling [3].

The study of brain structure has been driven by the analysis of medical images. Specifically, neuroimaging has been used to conduct quantitative studies about the structure and functionality of the central nervous system. Magnetic resonance imaging (MRI) is one of the widely used types of neuroimaging, established as a valuable tool for diagnosing neurological diseases, and a great help when evaluating brain morphology, allowing both the evaluation of pathology associated with clinical or cognitive symptoms, and a differential diagnosis [4]. Through MRI it is possible to differentiate brain tissue structures such as white matter, gray matter, and cerebrospinal fluid in tasks such as classification, identification, and segmentation [5-6]. The baseline for these tasks is done manually under the judgment and expertise of specialized physicians such as radiologists when performing a visual inspection of the images. However, performing this process manually poses challenges regarding the handling of large databases, biases, and mistakes associated with differences in contrast between images that pose a challenge even for experts due to the lack of consistent criteria. In recent years, brain MRI segmentation has been led by deep learning techniques [7]. This approach makes use of artificial neural networks with a large number of layers and neurons to extract a hierarchical structure of information from unprocessed input photos. Notable deep learning methods include stacking autoencoders, deep Boltzmann machines, deep neural networks, and convolutional neural networks, the latter of which is mostly used for image segmentation and classification.

The state of the art [8] employs deep learning algorithms to segment MRI structures in a variety of ways. One study developed a deep neural network architecture for autonomous segmentation and trained huge networks with tens of millions of parameters with little input, yielding encouraging validation results. In another study [9], they used Gaussian-type point spread functions, Richardson-Lucy (RL) deconvolution, intensity thresholding, connected component, and morphological operations to extract brain regions from coronal T1-W magnetic resonance images while improving border detection and picture quality. It recognized the brain boundaries more accurately than other methods [10]. In another study [11], distinguishing brain tissue from non-brain tissue was a significant challenge when segmenting the brain. They created a skull extraction algorithm combining image texture feature analysis and mathematical morphology. One texture feature map was a brain mask, while the other was a non-brain mask using this technique. The brain is then removed by morphological methods [12]. They also presented Atropos, an open-source multivariate n-class segmentation algorithm built on the Insight Toolkit. This method was developed using expectation-maximization (EM) algorithms with parametric or nonparametric finite mixtures to model class intensities [13]. In addition, they used spatial prior probability maps, previous label maps, and MRF modeling. Using a series of training segmentations, "SynthSeg" created synthetic scans of extraordinarily varied contrasts on the fly during training [14]. To segment each data contrast, these scans used the generative model of classical Bayesian segmentation with randomly generated parameters for appearance, deformation, noise, and bias field, which performed slightly better than classical Bayesian segmentation and was three orders of magnitude faster. Finally, Zhao (2022) [15] proposed "MixNet", a 2D semantic deep convolutional neural network that differentiates brain structure in multimodal magnetic resonance images by replacing the typical convolutional layer with a dilated one, omitting

pooling and deconvolutional layers, and decreasing network parameters. With only four participants to train, they achieved 84.7% Dice coefficients for gray matter, 87.3% for white matter, and 83.4% for cerebrospinal fluid.

In this work, a convolutional neural network (CNN), based on the U-Net architecture is presented for the segmentation of brain MRI images and volumes, obtaining segmented images with labels corresponding to: background, gray matter, white matter, and cerebrospinal fluid. Subsequently, the results obtained are compared with other MRI segmentation methods used as Dipy and the FAST method from the FMRIB Software Library (FSL) using four performance metrics. The results show that MRI image segmentation using convolutional networks, specifically 2D U-Net and 3D U-Net networks, are more effective than the other implemented methods, offering better performance for segmenting brain structures without the need to resort to external modules or software.

2. Methodology

Figure 1 presents the methodological scheme for MRI analysis, which includes the following steps. The performance of clinical studies for image acquisition, the formation of a database on specific conditions to be treated, that is, the diseases or deformities existing in patients, and the analyses performed by the expert medical team that determine the clinical conditions that are then used as labels to train the models. In this work, the use of deep learning models is proposed in the machine learning stage, specifically the U-Net network that has been previously mentioned. With the training of the models, validation is then carried out with the test dataset. The objective of this study is the accurate segmentation of the focal area (gray matter and white matter), avoiding highlighting other areas. Finally, the general scheme includes model evaluation, in this case, metrics that determine the similarity between the model's segmentation and the segmentation given by the expert were used.

2.1. Medical Image Acquisition Methods

There are various medical image acquisition technologies, from obtaining images using X-rays to modern multimodal devices. Among these technologies, six of them can be found as the most recognized in general, starting with ultrasound, X-rays, tomography, MRI, Gamma camera and finally fluoroscopy.

MRI stands out as a very powerful tool for anatomical diagnosis due to its high spatial resolution and because it is non-invasive; which makes it an exam par excellence for the study of medical images. MRI allows generating three-dimensional anatomical images in grayscale, which is a great advantage when processing them.

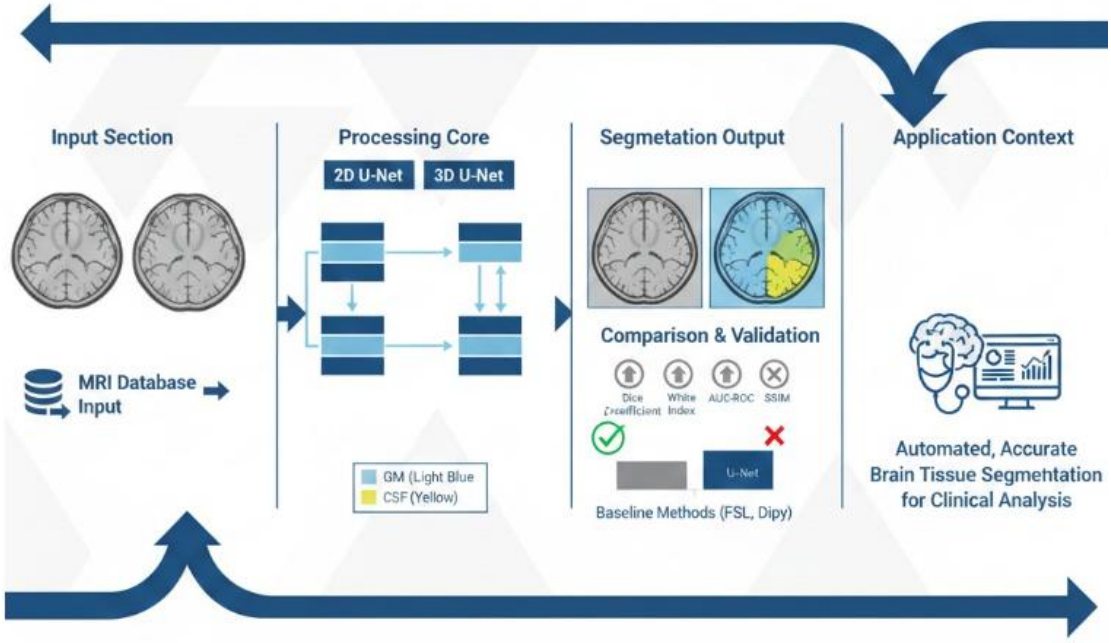

Fig. 1 *Proposed methodological structure for magnetic resonance image segmentation based on deep learning.*

2.2. Convolutional Neural Network (CNN)

Convolutional neural networks (CNNs) are a type of artificial neural network frequently used for image analysis and recognition. These networks are highly effective in computer vision tasks, such as image classification and segmentation, where unlike conventional neural networks that use linear operations between layers to obtain representations of the inputs, CNNs use convolutional layers, and as the input passes through each of the layers, they apply filters to the image that manage to abstract nonlinear information from the analyzed pixels, generating discriminatory features [16].

Conventional neural networks are fully connected (FC), that is, all neurons in a hidden layer are connected to all neurons in the preceding and succeeding layers. This process generates a huge number of parameters (also known as the network weights), because each layer that the network has will have each neuron connected to each other, and in turn, these neurons in each layer will connect to each pixel of the image, which would be a problem when training a network with a considerable volume of images, causing unfeasibility due to the enormous number of weights that would be obtained.

Convolutional neural networks emerged as an alternative solution to the above. These networks have convolutional and pooling layers that alternate and end with FC layers. A convolutional layer consists of filters or kernels of size f × f × c each, where c refers to the depth or number of channels (3 for color images, 1 for grayscale images). Additionally, a pooling layer is usually introduced at the output of a convolution that reduces the size of the images by performing the corresponding grouping operation, commonly maximum or average ("MaxPooling" or "AvgPooling") [17].

Within convolutional neural networks, multiple CNN network architectures have been successfully developed that have achieved outstanding results in different areas. Some of

them are LeNet, AlexNet, VGGNet, U-Net, GoogLeNet, among others. Of these, the U-Net architecture will be used to develop the medical image and volume segmentation algorithm.

2.3. U-Net Architecture

The U-Net architecture is a convolutional network designed for rapid and precise segmentation of medical images. There exist two U-Net architectures; the initial architecture is the 2D U-Net network, which comprises a contracting path adhering to the conventional structure of a convolutional network, featuring 3 × 3 convolutions, rectified linear units (ReLU), and 2D MaxPooling operations, alongside an expanding path that entails upsampling the feature map, succeeded by 2 × 2 convolutions ("up-convolution") that reduce the channel count by half, and 3 × 3 convolutions, each accompanied by a ReLU. The network comprises 23 convolutional layers. The second design is the 3D U-Net network, which utilizes the entire volume (or subvolumes) and employs three-dimensional convolutional layers together with three-dimensional maximum pooling operations (MaxPooling 3D) for both the contracting and expanding paths [18-19].

2.4. Other MRI Segmentation Methods

Dipy is an external library compatible with Python, enabling its installation and utilization as a tool for magnetic resonance image analysis. This library executes segmentation of three tissues mostly via Bayesian formulation. The observation model is characterized by a Gaussian distribution, while a Markov random field (MRF) is employed to represent the prior probability of context-dependent patterns of various brain tissue types. Expectation maximization and iterative conditional modes are employed to ascertain the ideal solution [20].

FSL is a toolkit for the study of fMRI, MRI, and DTI brain imaging data. Its functionalities can be accessed via both graphical user interface (GUI) and command line. The library includes an algorithm for brain extraction from resonance pictures, known as BET (Brain Extraction Tool), which employs a deformable model that adapts to conform to the brain surface via a series of adaptive local models. The FAST algorithm (FMRIB's Automated Segmentation Tool from the University of Oxford) in this collection segments several tissue types in 3D brain pictures via a method grounded in Markov random fields and a corresponding expectation maximization algorithm.

2.5. Performance Measures

1. Dice Coefficient: also known as the Sorensen similarity index can be used in the field of information retrieval and in other areas. The dice coefficient measures the similarity between sets, as indicated in equation (1).

$$\boldsymbol{DC = \frac{2 \mid A \cap B \mid}{\mid A \mid + \mid B \mid}} \textbf{ equation } (\mathbf{1}).$$

where A is the set of ground truth, while B signifies the computed segmentation. Both images (sets) are binary, containing values of 0 or 1 in each of their voxels or pixels in the two-dimensional instance.

2. Jaccard Index: the Jaccard index measures similarity in terms of the relationship between the intersection and union of two sample sets, as indicated in equation (2).

$$\boldsymbol{J = \frac{|A \cap B|}{|A \cup B|}} \textbf{ equation (2).}$$

3. The Area Under the Curve (AUC) of the ROC curve is a valuable and commonly utilized metric for assessing the performance of binary and multi-class classification algorithms. Nonetheless, it does not consider the precise numerical output of the models; instead, it examines how the output categorizes the cases, so enabling the representation of the classifier's performance as a singular value.

$$\boldsymbol{AUC = \frac{1}{2}(TPR - FPR + 1)} \quad \textbf{equation (3)}$$

where True Positive Rate (TPR) represents the correct positive predictions among the total number of po

4. Structural Similarity (SSIM): SSIM is an image fidelity measure that has proven to be very effective for measuring signal fidelity.

3. Experimental Framework

3.1. Databases

A search for multiple brain databases in different repositories, web pages, and challenges related to MRI segmentation was conducted. Mainly, public databases that had a large number of images and age heterogeneity were examined, as this would guarantee better results in network training. Finally, three MRI segmentation databases were chosen, which are presented below:

1. The first database was extracted from the challenge, which contains twenty 3T magnetic resonance brain scans of patients over 50 years of age, with diabetes and matched controls of various degrees of atrophy and white matter lesions. This database is divided into five datasets (MRI scans with manual segmentations) for training and fifteen datasets (only MRI scans) for testing. In our case, only the five training datasets are of interest, specifically the T1-weighted images of each dataset, as these contain their own manual segmentation performed by an expert. The manual segmentations consist of eight labels from 1 to 8, corresponding to a different brain tissue, but only labels 1, 3, and 5 were of interest, corresponding to gray matter (GM), white matter (WM) and cerebrospinal fluid (CSF), respectively. The additional labels were taken as background in each of the tests.

For each patient, the subsequent sequences are supplied:

- T1_1mm: T1-weighted three-dimensional scan (voxel dimensions: 1.0mm × 1.0mm × 1.0mm)
- T1: T1-weighted three-dimensional scan aligned with T2 FLAIR (voxel dimensions: 0.958 mm × 0.958 mm × 3.0 mm)

- T1_IR: Multislice T1-weighted inversion recovery scan aligned with T2 FLAIR (voxel dimensions: 0.958 mm × 0.958 mm × 3.0 mm)
- T2_FLAIR: multi-slice FLAIR scan (voxel dimensions: 0.958 mm × 0.958 mm × 3.0 mm)

2. MRBrainS18: The second database was extracted from the challenge, which contains scans of 30 patients over 50 years of age with diabetes, dementia, Alzheimer's and matched controls (with higher cardiovascular risk) of various degrees of atrophy and white matter lesions. These data consist of 7 sets of brain MRI images. For our study, the T1-weighted images of each dataset are of interest, as these contain their own manual segmentation performed by an expert. The manual segmentations consist of eleven labels from 0 to 10, corresponding to a different brain tissue, but only labels 1, 3, and 5 were of interest, corresponding to GM, WM and CSF, respectively. The additional labels were taken as background in each of the tests.

   For each patient, the subsequent sequences are supplied:

   - T1: T1-weighted 3D sequence (voxel size: 0.958 mm × 0.958 mm × 3.0 mm)
   - T1-IR: Multiclice T1-weighted inversion recovery sequence (voxel size: 0.958 mm × 0.958 mm × 3.0 mm)
   - T2-FLAIR: Multiclice T2 FLAIR sequence (voxel size: 0.958 mm × 0.958 mm × 3.0 mm)

3. Internet Brain Segmentation Repository (IBSR): This is a brain MRI database that includes manually guided segmentations by an expert in order to develop and evaluate segmentation methods. The volumes were placed in the public domain by Rohlfing and can be obtained at http://www.nitrc.org/.

   The database includes studies of 18 patients of which 4 are women and 14 men with ages ranging from 7 to 71 years. For each patient, T1 sequence MRIs with and without skull, brain mask, and segmentations of brain structures are found. The volumes have a resolution of 256 × 256 × 128 px and a voxel size of 0.938 × 0.938 × 1.5 mm.

   Figure 2 shows an example of each of the T1 volumes from the selected databases, which also shows the manual segmentations of the brain tissues of our interest: Gray Matter (GM) and White Matter (WM).

   The three datasets were standardized to a common space of dimension 240 × 240 × 48, seeking to avoid filtering of information that affects the validity of the results obtained by the proposed methods.

3.2. Methods

Using the databases described above, the proposed segmentation method was implemented, for which two variants were presented, one based on two-dimensional representations of the images (U-Net 2D) and the other using 3D images. These methods were compared with two established methodologies in the state of the art in order to demonstrate progress in the segmentation task.

1. Segmentation using convolutional networks: The first method consists of creating a convolutional network based on the U-Net architecture, to segment magnetic resonance images in 2 and 3 dimensions; in both cases, four of the five MRIs with manual segmentations provided by the MRBrainS13 dataset were used for training, the remaining MRI will be used to evaluate the trained networks and comparison techniques. For the 2D U-Net, in the contraction stage, images with dimensions of 240 × 240 × 1 are input, referring to the fact that they are 2D grayscale images, followed by two convolutions of 16 filters each

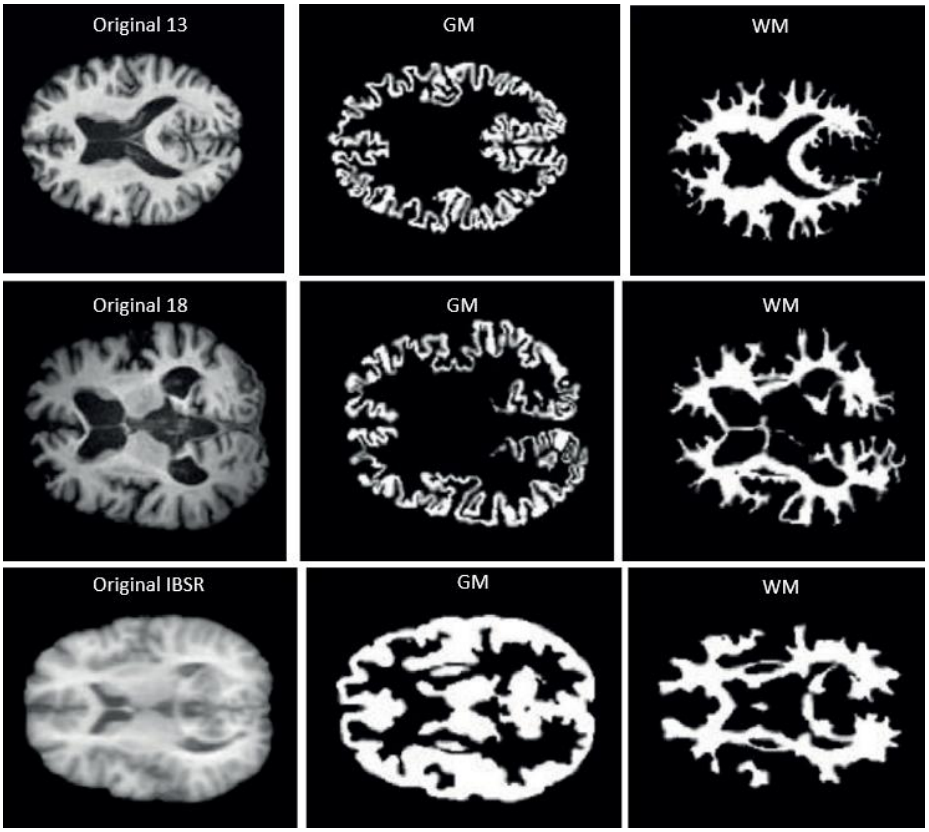

Fig. 2 *Example view of a brain for each database and their corresponding manual segmentations of gray matter and white matter*

to begin extracting features from the image. Finally, a MaxPooling is applied to reduce similar features and at the same time, halve the size of the resulting image.

Then, this same procedure of two convolutions and a MaxPooling is applied for three different levels of the network, but the variation is that, at each subsequent level, double the filters of the previous level are applied in each convolution, that is, in the first level 16 filters were applied to the image, then, in the next level 32 filters will be applied, and so on for the other levels until reaching the bottom of the network, where 2 convolutions of 256 filters are performed without MaxPooling to extract more precise features.

After this last contraction stage, the expansion stage begins, which aims to return the image to its original size. Here the inverse process of convolution is applied, i.e., transposed convolution, which basically performs padding on the original image followed by some convolutional layers, applying the same filters as the contraction stage, but in descending order. In turn, after applying the transposed convolution, the image is also

concatenated with the corresponding image from the contraction path, with the aim of using the features extracted there. This process mentioned above, is executed for 3 more levels of the expansion stage up to the last level of the network, where a final convolutional layer with a filter of size 1 × 1 is performed to meet the prediction requirements. The complete network scheme can be seen in Figure 3.

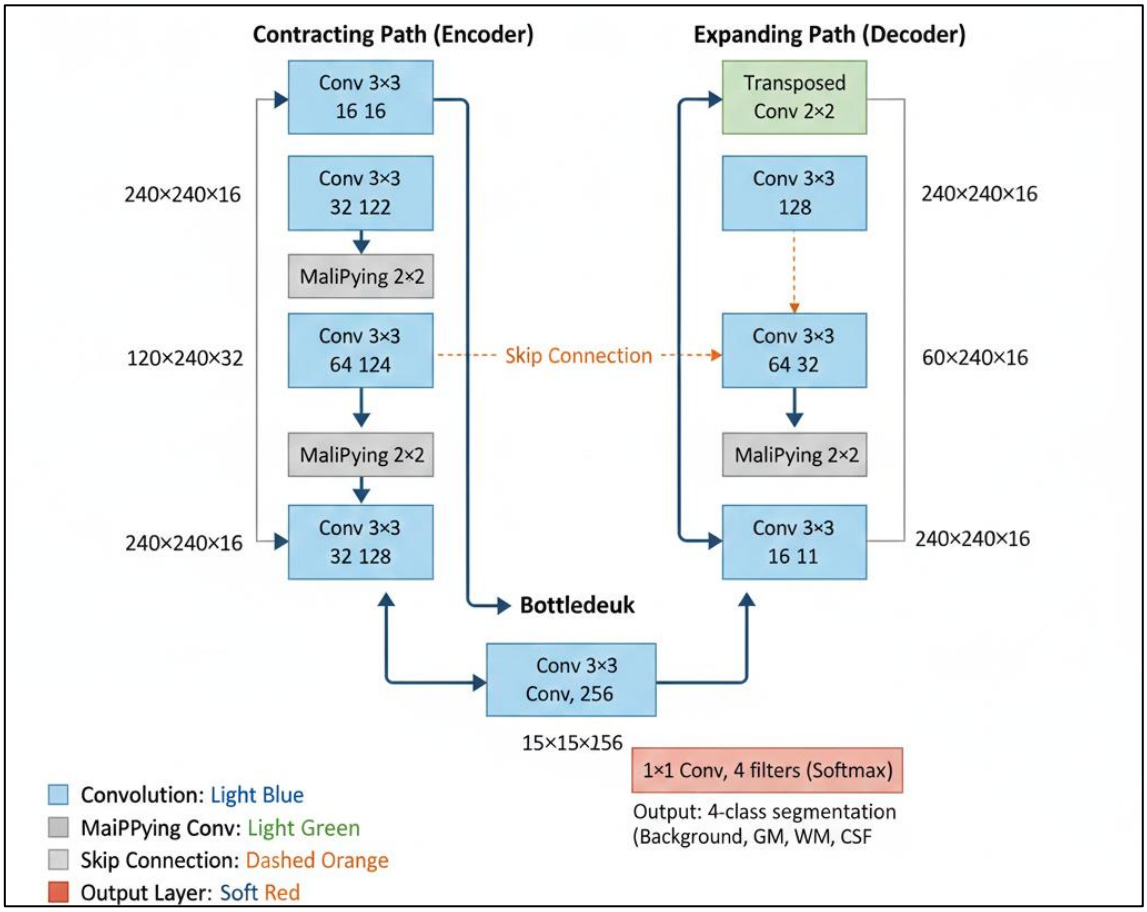

Fig. 3 *Architecture of the 2D U-Net network*

After building the 2D U-Net network, preprocessing of the database images is performed, in order to have standard images, with the corresponding data type and correct dimensions to proceed with their training. For the 3D U-Net network, subvolumes of size 80 × 80 × 16 were used, in order to synthetically increase the total number of training data, reduce the computational cost of the network and the total number of parameters. The same number of filters were used in each layer as in the 2D U-Net network in its three-dimensional version.

The Adam optimizer was employed during the network training process, with a learning rate of 0.001, β1 set to 0.9, and β2 set to 0.999. The employed loss function was binary cross-entropy, and a total of 100 epochs were executed, retaining the optimal training epoch based on accuracy results.

2. Segmentation using FSL: This method is presented as the first comparison technique. FSL is a library for statistical analysis of fMRI, MRI and DTI, in this case, the module for brain tissue segmentation into gray matter (GM), white matter (WM) and CSF was used. For parameterization, separate output of binarized images for each tissue type

was used, partial volume estimation was performed, 3 output classes corresponding to the tissues of interest were selected and NIFTI type outputs were used. Additionally, for the input image type, T1 was used, which indicates that T1 contrast is maximized.

3. Segmentation using Dipy: For this method it must be taken into account that the magnetic resonance images must be without the skull, otherwise, additional processing must be performed where the non cerebral part of the images is removed, in order to obtain better results in the segmentation.
   After verifying the above, some important parameters are adjusted such as the number of classes, which for this case are 3: GM, WM and CSF. Also, the image smoothing factor called beta, which helps eliminate noise points from them. This parameter ranges between 0 and 0.5, which for our case was defined at 0.1, as this is where it achieves better performance. Another parameter that can also be redefined is the number of iterations, since by default this is 100, however, it is possible to reach convergence in fewer iterations depending on the model, so it is not necessary to reach or exceed that number of iterations in some cases, so it was determined to adjust it for a total of 20 iterations.
   After assigning the parameters defined above, an instance of the "TissueClassifierHMRF" class is created with its respective "classify" method for the magnetic resonance images, where at the end, after the assigned number of iterations, the image with the expected labels of each brain tissue will be obtained.
   Seeking to guarantee the reproducibility of this study, the codes for training and using the proposed methods and baseline methods can be found in the following repository: https://github.com/JovianPlanet/brain_segmentation.

4. Results & discussion

After training the presented U-Net architectures, evaluation of both the proposed models and the comparative methods was carried out. In this stage, evaluation metrics based on set theory, the area under the curve (AUC) and SSIM which is based on structural similarity of images were used. Thus, the statistical results and examples of the models' performance for segmenting both gray matter and white matter are shown below.

Initially, Figure 4 presents the results obtained for gray matter segmentation using a box diagram (boxplot). For these results, the performances evaluated with the four implemented metrics are shown. The results show that, for each evaluation method, the proposed architectures (2D U-Net and 3D U-Net) manage to achieve scores above 0.9 in most metrics, except for the Jaccard score, which for all analyzed methods presents a significant drop. However, U-Net-based methods for the Jaccard score maintain a median close to 0.8, while for the comparison methods the median is lower than 0.6 in the case of FSL and lower than 0.4 for Dipy. In general, it can be said that for gray matter segmentation, the methods proposed in this work maintain a variance lower than the methods with which they are compared. In addition, they have a higher median and less variation of results between the different metrics.

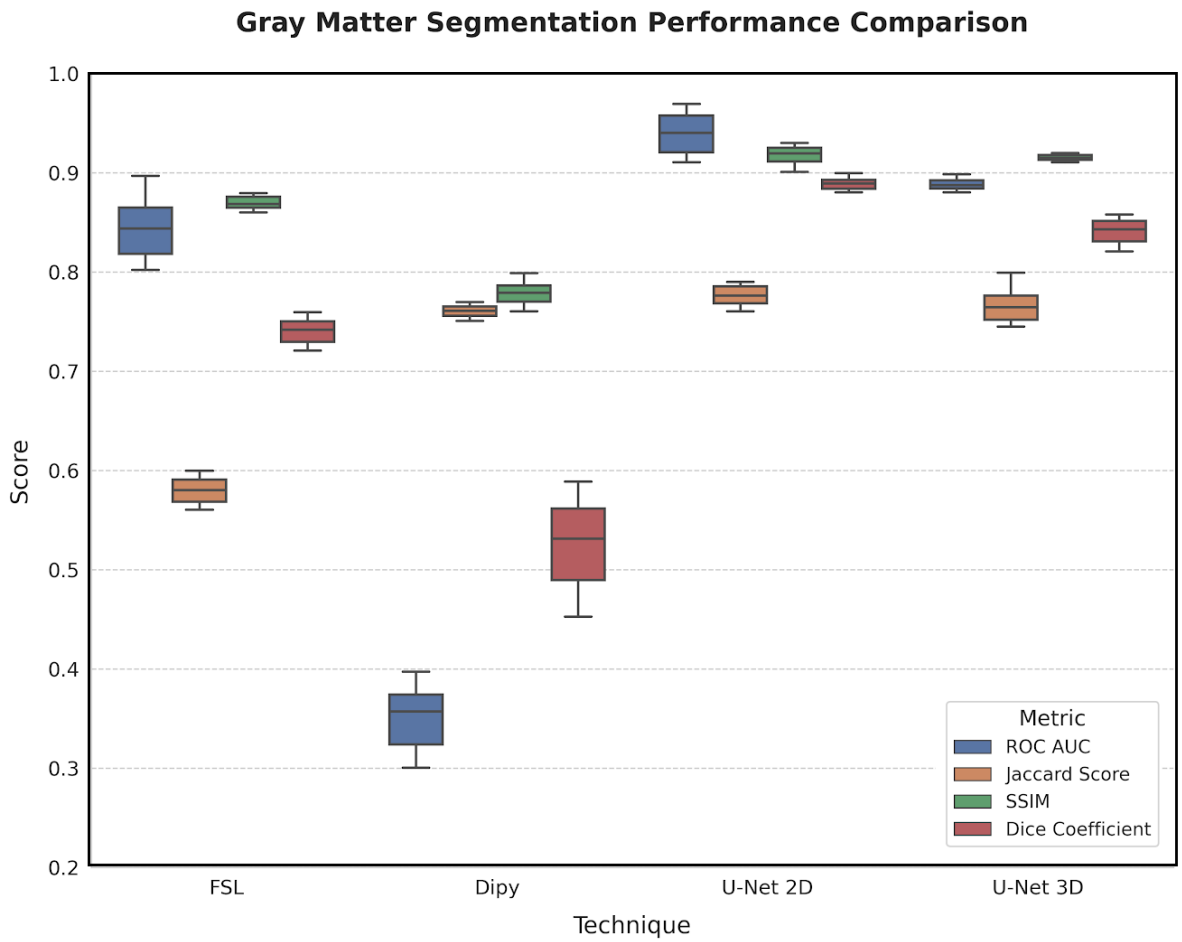

Fig. 4 *Comparison of results for gray matter segmentation*

Additionally, Figure 5 shows some results as an example of the segmentation performed by the proposed techniques and comparison methods on a volume from the MRBrainS18 dataset. In white, the ground truth is presented, and on it, using transparency, the delineation obtained by each method. The figure shows that U-Net in both versions manages to follow the grooves of the analyzed structure, while for the other methodologies ventricles are also marked. On the other hand, it is visually perceived that the regions of convergence between the real label and the outputs of the methods using U-Net are greater than those obtained by FSL and Dipy. This can be seen in the white spaces that remain inside the structure, being more noticeable in Dipy than FSL.

Figure 6 presents the results of the box diagram obtained for white matter segmentation. These results show, unlike gray matter, lower variability between the different methods and evaluation metrics, finding that the average of the scores remains above 0.6, while for gray matter they could be below 0.4, which suggests that white matter segmentation is a less demanding task than gray matter segmentation. As in the previous experiment, the proposed methods continue to have a high median in the score for each metric. In the case of the Jaccard score, as with gray matter, a significant decrease in the median and greater variance is noted in all methods, although the drop remains smaller for U-Net-based methods.

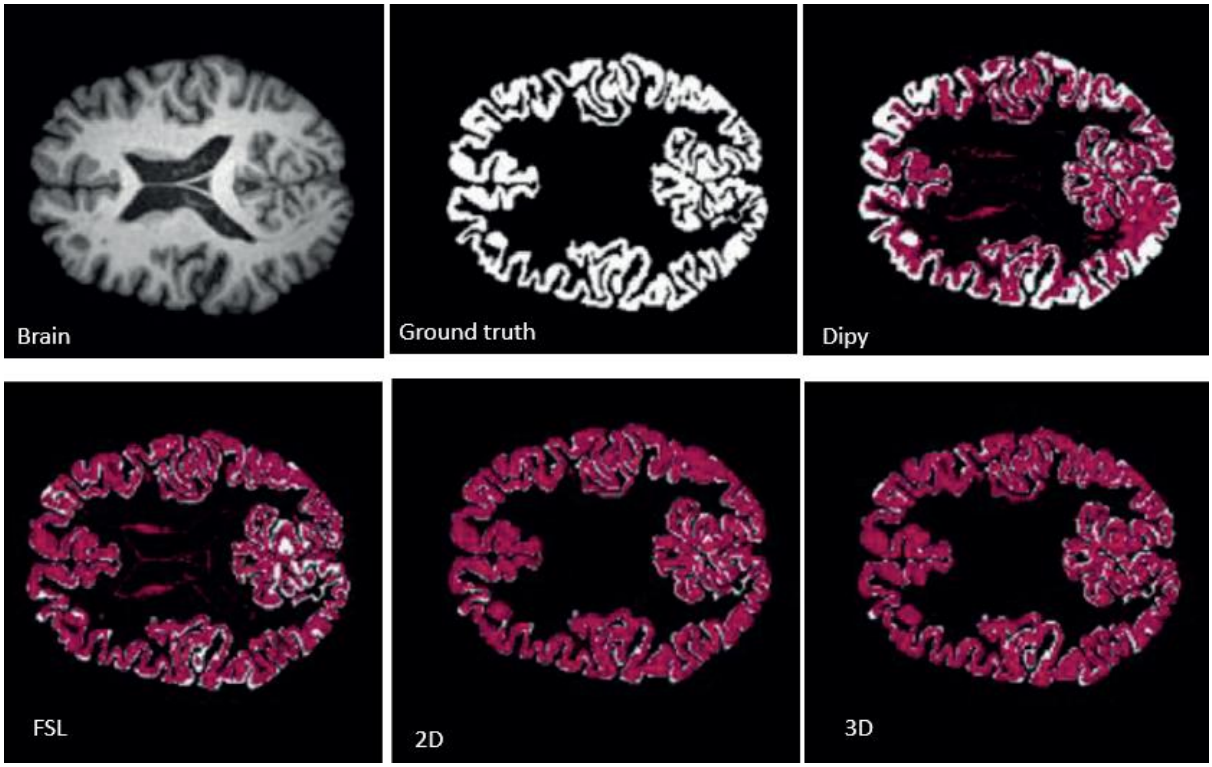

Fig. 5 *Example result for gray matter segmentation on MRBrainS18 volume.*

Finally, an example of white matter segmentation on a volume from the IBSR dataset is shown in Figure 7. The results for the contemplated techniques are presented, in white the comparison label (Ground truth) is presented, and on this, using transparency, the delineation obtained by each method. In this case the results are consistent with what was reported in the previous experiment, where Dipy presents a large number of unsegmented tissue spaces and FSL, although it performs better segmentation, makes erroneous marking on components that are outside the structure of interest. On the other hand, when analyzing U-Net, it can be seen how the unsegmented spaces are reduced (similar for both proposals) and also there is less marking of areas outside the structure, where better performance can be evidenced when the 2D model is used.

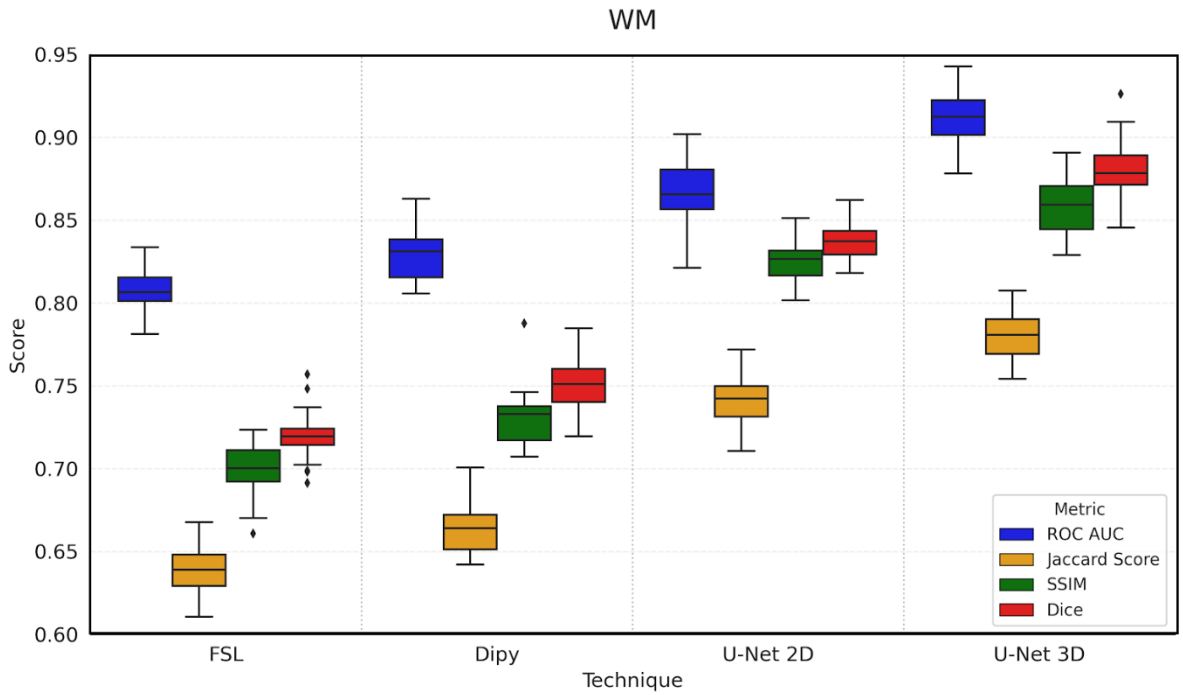

Fig. 6 *Comparison of results for white matter segmentation*

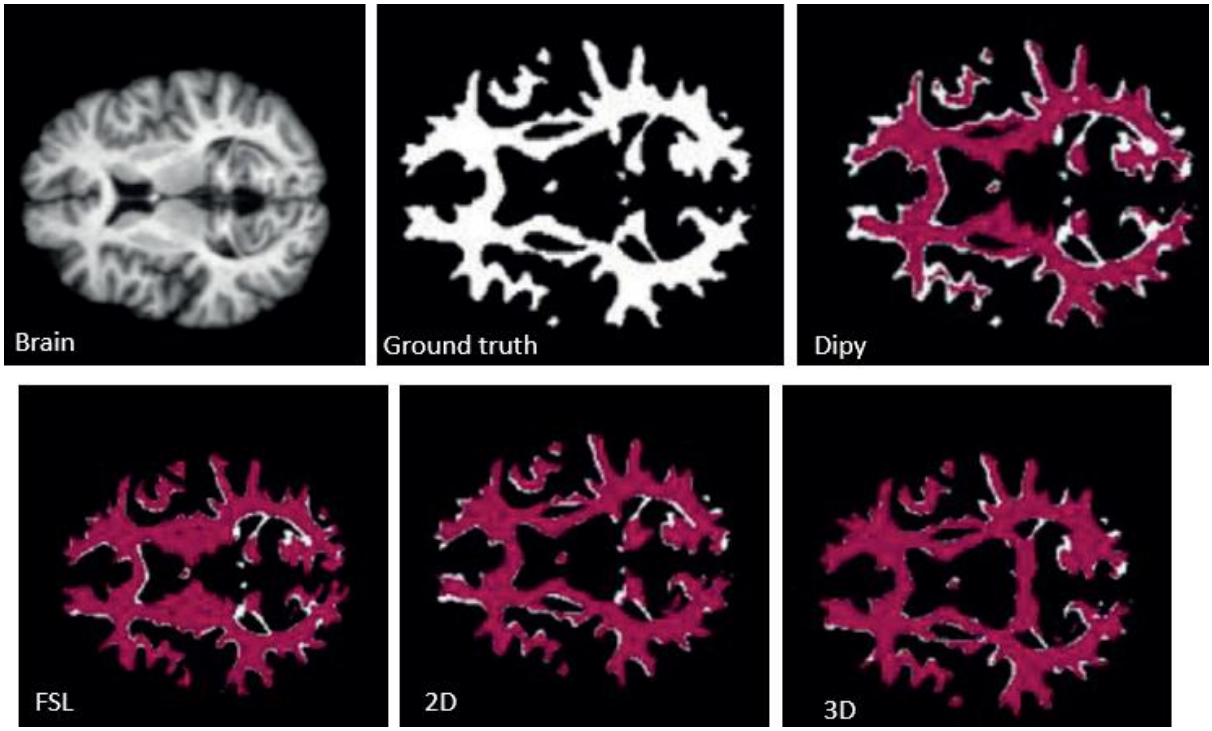

Fig. 7 *Example result for white matter segmentation on IBSR volume*

5. Conclusions

In this work, a brain tissue segmentation technique using neural network architectures was proposed, specifically working with U-Net networks in two different versions that received images in 2D or volumes in 3D. The results of this research show how the proposed technique manages to improve the performance of the gray and white matter segmentation task when compared with recent state-of-the-art methodologies. In general, it was evident that the U-Net architectures significantly reduce the segmentation of components outside the tissues of interest, that is, there is less segmentation of the surrounding tissues.

When comparing the 2D and 3D model, it can be concluded that the 2D model is slightly superior to the 3D one when looking at the box diagrams in all evaluation measures. Additionally, when looking at the segmentation areas, it can be seen how the 2D model decreases the unsegmented areas mainly for gray matter, and for white matter, segmentations outside the tissue are reduced. In general, the 2D model reduces both false positives and false negatives of the segmentation.

The main challenge for the proposed methodology to be used online is found in the training stage, due to the iterative tuning of parameters. Subsequently in the evaluation stage, the computation speed decreases considerably to be used in real time. However, it is important to consider that the MRIs to be used must be brought to the input space of the networks, that is, 240 × 240 × 48, which allow individual use on the axial axis for the 2D model and the use of sub volumes of dimension 80 × 80 × 16 in the 3D model.

As future work is to validate the performance of the proposed architecture in other brain structures to evaluate the generalization of the model. On the other hand, although there is a noticeable improvement in the segmentation task, there are still contours that are difficult to distinguish for the model, which establishes a work route in order to implement improvements that allow the segmentation of zones that seem to be challenging for the different implemented techniques.

References

[1]. Gaitanis J, Tarui T. Nervous System Malformations. *Continuum (Minneap Minn)*. 2018;24(1, Child Neurology):72–95. doi:10.1212/CON.0000000000000561

[2]. Blinkouskaya Y, Weickenmeier J. Brain Shape Changes Associated With Cerebral Atrophy in Healthy Aging and Alzheimer's Disease. *Front Mech Eng*. 2021;7:705653. doi:10.3389/fmech.2021.705653

[3]. Ineichen BV, Cananau C, Plattén M, Ouellette R, Moridi T, Frauenknecht KBM, et al. Dilated Virchow-Robin Spaces are a Marker for Arterial Disease in Multiple Sclerosis. *bioRxiv* [Preprint]. 2023 Feb 27:2023.02.24.529871. doi:10.1101/2023.02.24.529871

[4]. Gorgolewski K, Auer T, Calhoun V, et al. The brain imaging data structure, a format for organizing and describing outputs of neuroimaging experiments. *Sci Data*. 2016;3:160044. doi:10.1038/sdata.2016.44

[5]. Yen C, Lin CL, Chiang MC. Exploring the Frontiers of Neuroimaging: A Review of Recent Advances in Understanding Brain Functioning and Disorders. *Life (Basel)*. 2023;13(7):1472. doi:10.3390/life13071472

[6]. Narayana PA, Coronado I, Sujit SJ, Wolinsky JS. Deep learning-based neural tissue segmentation of MRI in multiple sclerosis: Effect of training set size. *J Magn Reson Imaging*. 2020;51(5):1487–1496

[7]. Ye Z, George A, Wu AT, Niu X, Lin J, Adusumilli G, et al. Deep learning with diffusion basis spectrum imaging for classification of multiple sclerosis lesions. *Ann Clin Transl Neurol*. 2020;7(5):695–706

[8]. Arab A, Chinda B, Medvedev G, et al. A fast and fully-automated deep-learning approach for accurate hemorrhage segmentation and volume quantification in non-contrast whole-head CT. *Sci Rep*. 2020;10:19389. doi:10.1038/s41598-020-76459-7

[9]. Guo S, Lu Y, Li Y. Richardson–Lucy Iterative Blind Deconvolution with Gaussian Total Variation Constraints for Space Extended Object Images. *Photonics*. 2024;11(6):576. doi:10.3390/photonics11060576

[10]. Dell'Acqua F, Tournier JD. Modelling white matter with spherical deconvolution: How and why? *NMR Biomed*. 2019;32(4):e3945. doi:10.1002/nbm.3945

[11]. Verma A, Shivhare SN, Singh SP, et al. Comprehensive Review on MRI-Based Brain Tumor Segmentation: A Comparative Study from 2017 Onwards. *Arch Computat Methods Eng*. 2024;31:4805–4851. doi:10.1007/s11831-024-10128-0

[12]. Ranjbarzadeh R, Bagherian Kasgari A, Jafarzadeh Ghoushchi S, et al. Brain tumor segmentation based on deep learning and an attention mechanism using MRI multi-modalities brain images. *Sci Rep*. 2021;11:10930. doi:10.1038/s41598-021-90428-8

[13]. Panić B, Klemenc J, Nagode M. Improved Initialization of the EM Algorithm for Mixture Model Parameter Estimation. *Mathematics*. 2020;8(3):373. doi:10.3390/math8030373

[14]. Billot B, Greve DN, Puonti O, Thielscher A, Van Leemput K, Fischl B, Dalca AV, Iglesias JE; ADNI. SynthSeg: Segmentation of brain MRI scans of any contrast and resolution without retraining. *Med Image Anal*. 2023;86:102789. doi:10.1016/j.media.2023.102789

[15]. Zhao L, Ma J, Shao Y, Jia C, Zhao J, Yuan H. MM-UNet: A multimodality brain tumor segmentation network in MRI images. *Front Oncol*. 2022;12:950706. doi:10.3389/fonc.2022.950706

[16]. Taye MM. Theoretical Understanding of Convolutional Neural Network: Concepts, Architectures, Applications, Future Directions. *Computation*. 2023;11(3):52. doi:10.3390/computation11030052

[17]. Zhao X, Wang L, Zhang Y, et al. A review of convolutional neural networks in computer vision. *Artif Intell Rev*. 2024;57:99. doi:10.1007/s10462-024-10721-6

[18]. Yao W, Bai J, Liao W, Chen Y, Liu M, Xie Y. From CNN to Transformer: A Review of Medical Image Segmentation Models. *J Imaging Inform Med*. 2024;37(4):1529–1547. doi:10.1007/s10278-024-00981-7

[19]. Yousefi T, Aktaş Ö. New hybrid segmentation algorithm: UNet-GOA. *PeerJ Comput Sci*. 2023;9:e1499. doi:10.7717/peerj-cs.1499

[20]. Akan T, Oskouei AG, Alp S, et al. Brain magnetic resonance image (MRI) segmentation using multimodal optimization. *Multimed Tools Appl*. 2025;84:16971–17020. doi:10.1007/s11042-024-19725-4

IRAQI Academic Scientific Journals
Samarra Journal of Pure and Applied Science
SJPAS
مجلة سامراء للعلوم البحتة والتطبيقية
www.sjpas.com
p ISSN: 2663-7405
e ISSN: 2789-6838

إطار معلوماتي صحي ذكي لتقسيم أنسجة الدماغ آليًا في التصوير بالرنين المغناطيسي باستخدام الشبكات العصبية الالتفافية القائمة علىU-Net

مهند فاضل جويد
كلية الحضارة الجامعة/صلاح الدين العراق

معلومات البحث:
تأريخ الاستلام:09/01/2026
تاريخ التعديل: 20/02/2026
تأريخ القبــول: 15/03/2026
تاريخ الـنشر:10/04/2026
الكلمات المفتاحية:
التصوير بالرنين المغناطيسي للدماغ، تجزئة الأنسجة، شبكة يو-نت، الشبكات العصبية الالتفافية، تحليل الصور الطبية، التعلم العميق.

معلومات المؤلف
الايميل:
Mohanad02jwaid@gmail.com
الموبايل:

الخلاصة:

تقترح هذه الدراسة إطار عمل ذكيًا لتقسيم أنسجة الدماغ آليًا في صور الرنين المغناطيسي باستخدام الشبكات العصبية الالتفافية القائمة على U-Net، بهدف تحسين الدقة مقارنةً بالأساليب الحالية. تتضمن المنهجية تطبيق بنيتي U-Net ثنائية وثلاثية الأبعاد، تم تدريبهما والتحقق من صحتهما على مجموعات بيانات عامة (MRBrainS13، MRBrainS18، IBSR) مع تقسيمات يدوية من قبل خبراء. تمت مقارنة الأداء مع أدوات راسخة (FSL، Dipy) باستخدام معامل دايس، ومؤشر جاكارد، ومساحة تحت المنحنى (AUC)، ومؤشر التشابه الهيكلي (SSIM). تُظهر النتائج تفوق نماذج U-Net، حيث تجاوزت درجات دايس 0.9 للمادة الرمادية، مما يدل على اتساق عالٍ، بينما تفوقت U-Net ثنائية الأبعاد بشكل طفيف على نظيرتها ثلاثية الأبعاد في تقليل النتائج الإيجابية والسلبية الخاطئة. يؤكد الاستنتاج أن التقسيم القائم على U-Net يُحسّن بشكل كبير الدقة والموثوقية في تمييز المادة الرمادية والمادة البيضاء والسائل النخاعي، مما يوفر بديلاً قويًا للتقنيات التقليدية.